Acta Mechanica 86, 31–52 (1991)

ACTA MECHANICA

Dynamic shear band development in a thermally softening bimetallic body containing two voids

R. C. Batra and Z. G. Zhu, Rolla, Missouri

(Received May 18, 1990; revised July 12, 1990)

Summary. We study the development of shear bands in a thermally softening viscoplastic prismatic body of square cross-section and containing two symmetrically placed thin layers of a different viscoplastic material and two elliptical voids with their major axes aligned along the vertical centroidal axis of the cross-section. One tip of each elliptical void is abutting the common interface between the layer and the matrix material. Two cases, i.e., when the yield stress of the material of the thin layer in a quasistatic simple compression test equals either five times or one-fifth that of the matrix material are studied. The body is deformed in plane strain compression at an average strain-rate of 5,000 $\sec^{-1}$, and the deformations are assumed to be symmetrical about the centroidal axes.

It is found that in each case shear bands initiate from points on the vertical traction free surfaces where the layer and the matrix materials meet. These bands propagate horizontally into the layer when it is made of a softer material and into the matrix along lines making an angle of $\pm 45°$ with the vertical when the layer material is harder. In the former case, the band in the layer near the upper matrix/layer interface bifurcates into two bands, one propagating horizontally into the layer and the other into the matrix material along the direction of the maximum shear stress. The band in the layer near the lower matrix/layer interface propagates horizontally first into the layer and then into the matrix material along the direction of the maximum shear stress. Irrespective of the value of the yield stress for the layer material, a band also initiates from the void tip abutting the layer/matrix interface. This band propagates initially along the layer/matrix interface and then into the matrix material along a line making an angle of approximately 45° with the vertical.

1 Introduction

Johnson [1] has recently pointed out that Tresca [2] in 1878 and Massey [3] in 1921 observed hot lines, now referred to as shear bands, in the form of a cross during the hot forging of a metal. There has been a surge of activity in this area since the time Zener and Hollomon [4] reported 32 μm wide shear bands during the punching of a hole in a steel plate. They asserted that the heat generated because of the plastic working softened the material and that the material became unstable when thermal softening equalled the combined effects of strain and strain-rate hardening. The experimental observations of Moss [5], Costin et al. [6], Hartley et al. [7], Giovanola [8], and Marchand and Duffy [9] have added enormously to our understanding of the phenomenon of shear strain localization. Marchand and Duffy have pointed out that for thin steel tubes subjected to a pure torque at the ends, the localization of deformation into shear bands consists of three stages. In stage I, the body deforms homogeneously. In stage II, stipulated to initiate when the shear stress at a point attains its maximum value, the deformation becomes non-homogeneous. In stage III, that occurs much later, the shear stress drops precipitously and the deformation localizes into a shear band. These experimental observations agree with the numerical work of Wright and Walter [10], Molinari and Clifton [11], and Batra and Kim [12] to

[15]. We note that there have been numerous other numerical [16]—[24] and analytical studies [25]—[32] aimed at increasing our understanding of factors that affect the initiation and development of shear bands. These works have analysed the simple shearing deformations of a viscoplastic body containing a defect.

Recently, LeMonds and Needleman [33], [34], Needleman [35], Zbib and Aifantis [36], Anand et al. [37], Batra and Liu [38], [39], Zhu and Batra [40], and Batra and Zhang [41] have studied the phenomenon of shear banding in plane strain deformations of a viscoplastic solid. These works have generally used different constitutive relations and have assumed that the entire body or the portion of the body whose deformations were analyzed had only one defect in it. The prismatic body whose plane strain thermomechanical deformations are studied herein is of a square cross-section and has two thin layers made of a viscoplastic material different from that of the body and placed symmetrically about and parallel to the centroidal horizontal axis. These horizontal planes may be thought of as representing planes of chemical inhomogeneity. The material of the layer differs from that of the body only in the value σ_0 of the flow stress in a quasistatic simple compression test. Two cases, namely when σ_0 for the layer material equals five times or one-fifth that of the matrix material are studied. Also, there are two elliptical voids with major axes aligned with the vertical centroidal axis of the square cross-section and with tips touching the layer/matrix interfaces. The other ends of the ellipsoidal voids are towards the center of the cross-section. The points on the free edges where the thin layer and the matrix materials meet as well as the void vertices on the major axes of the ellipsoid act as nuclei for the initiation of shear bands. It thus becomes an interesting excercise to investigate the initiation and propagation of various bands and the interaction amongst them. We add that we do account for the effect of inertia forces, strain-rate sensitivity of the materials, their thermal softening, heat conduction, and the heat generated because of plastic working.

2 Formulation of the problem

The cross-section of the prismatic body containing two ellipsoidal voids and two thin layers of a different viscoplastic material is shown in Fig. 1. The deformations of the body are assumed to be symmetrical about the two centroidal axes. Thus, the deformations of the material in the first quadrant are analyzed. With respect to a fixed set of rectangular Cartesian coordinate axes, equations governing the plane strain thermomechanical deformations of the body are:

$$(\varrho J)^{\cdot} = 0, \tag{2.1}$$

$$\varrho_0 \dot{v}_i = T_{i\alpha,\alpha}, \tag{2.2}$$

$$\varrho_0 \dot{e} = -Q_{\alpha,\alpha} + T_{i\alpha} v_{i,\alpha}, \tag{2.3}$$

$$D_{ij} = (v_{i,j} + v_{j,i})/2, \tag{2.4}$$

$$T_{i\alpha} = (\varrho_0/\varrho)\, \sigma_{ij} x_{\alpha,j}, \qquad \sigma_{ij} = -B(\varrho/\varrho_0 - 1)\, \delta_{ij} + 2\mu D_{ij}, \tag{2.5}$$

$$2\mu = \left[\sigma_0/\left(\sqrt{3}\, I\right)\right] (1 + bI)^m\, (1 - \alpha\theta), \tag{2.6}$$

$$I^2 = (1/2)\, \bar{D}_{ij} \bar{D}_{ij}, \tag{2.7}$$

$$\bar{D}_{ij} = D_{ij} - (1/3)\, D_{kk} \delta_{ij}, \tag{2.8}$$

$$Q_\alpha = (\varrho_0/\varrho)\, q_i x_{\alpha,i}, \qquad q_i = -k\theta_{,i}, \tag{2.9}$$

$$\dot{e} = c\dot{\theta} + B(\varrho/\varrho_0 - 1)\, \dot{\varrho}/\varrho^2. \tag{2.10}$$

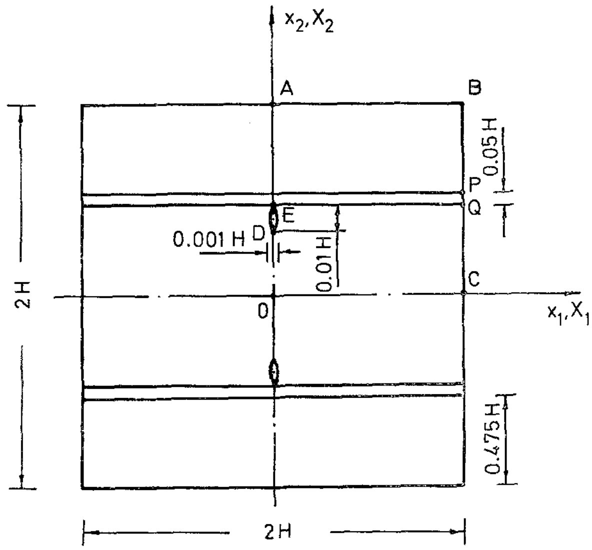

Fig. 1. The cross-section of the prismatic body studied

Equations (2.1), (2.2) and (2.3), written in terms of the referential description of motion, express respectively the balance of mass, balance of linear momentum and the balance of moment of momentum. Equations (2.5), (2.9) and (2.10) are the constitutive assumptions. In these equations x_i gives the position at time t of the material particle X_α, $v_i = \dot{x}_i$ is its velocity in the x_i-direction, ϱ is its present mass density, ϱ_0 its mass density in the reference configuration, $J = \det [x_{i,\alpha}]$, $x_{i,\alpha} = \partial x_i/\partial X_\alpha$, $T_{i\alpha}$ is the first Piola-Kirchhoff stress tensor, e is the specific internal energy, Q_α is the heat flux measured per unit area in the reference configuration, and $\boldsymbol{D}$ is the strain-rate tensor. Furthermore, a superimposed dot indicates material time derivative, a comma followed by index $\alpha(j)$ implies partial differentiation with respect to X_α (x_j), and a repeated index implies summation over the range (1, 2) of the index. In the constitutive relations (2.5), (2.9) and (2.10), the material parameter B may be regarded as the bulk modulus, σ_0 is the yield stress in a quasistatic simple compression test, parameters b and m describe the strain-rate hardening of the material, α is the thermal softening parameter, θ equals the temperature change of a material particle from that in the reference configuration, k is the thermal conductivity and c is the specific heat. Both k and c are taken to be constants and we have neglected stresses caused by the thermal expansion.

Equations (2.1) through (2.10) hold in the regions occupied by the matrix and the layer, the only difference being either

$$\sigma_0 \text{ layer} = 5\sigma_0 \text{ matrix}, \tag{2.11.1}$$

or

$$\sigma_0 \text{ layer} = (1/5)\, \sigma_0 \text{ matrix}. \tag{2.11.2}$$

The values of other material parameters are the same for the matrix and the layer.

With $\boldsymbol{s}$ defined by

$$\boldsymbol{s} = \boldsymbol{\sigma} + [B(\varrho/\varrho_0 - 1) - (2\mu/3) \operatorname{tr} \boldsymbol{D}]\, \mathbf{1}, \tag{2.12.1}$$

$$= 2\mu\overline{\boldsymbol{D}}, \tag{2.12.2}$$

equations (2.12), (2.5) and (2.6) give

$$(1/2 \operatorname{tr} \mathbf{s}^2)^{1/2} = \left(\sigma_0/\sqrt{3}\right)(1 - \alpha\theta)(1 + bI)^m. \tag{2.13}$$

This can be viewed as the equation of a generalized von Mises yield surface when the flow stress, given by the right-hand side of (2.13), at a material particle depends upon its strain-rate and temperature.

For the initial conditions we take

$$\varrho(\boldsymbol{x}, 0) = 1, \qquad \boldsymbol{v}(\boldsymbol{x}, 0) = \boldsymbol{0}, \qquad \theta(\boldsymbol{x}, 0) = 0. \tag{2.14}$$

That is, the body is initially at rest at a uniform temperature and has constant mass density. We also assume that the body is initially stress free. The pertinent boundary conditions for the material analyzed in the first quadrant are

$$v_2 = -h(t), \qquad T_{12} = 0 \quad \text{and} \quad Q_2 = 0, \quad \text{on the top surface } AB, \tag{2.15}$$

$$T_{11} = 0, \qquad T_{21} = 0 \quad \text{and} \quad Q_1 = 0, \quad \text{on the right surface } BC, \tag{2.16}$$

$$v_2 = 0, \qquad T_{12} = 0 \quad \text{and} \quad Q_2 = 0, \quad \text{on the bottom surface CO}, \tag{2.17}$$

$$v_1 = 0, \qquad T_{21} = 0 \quad \text{and} \quad Q_1 = 0, \quad \text{on parts } OD \text{ and } EA \text{ of the left surface } OA, \tag{2.18}$$

$$T_{i\alpha}N_\alpha = 0 \quad \text{and} \quad Q_\alpha N_\alpha = 0, \quad \text{on the surface } DE \text{ of the void}. \tag{2.19}$$

These boundary conditions simulate the situation when the top surface is moving downward with a speed $h(t)$, there is no friction between it and the loading device, the right surface is traction free, the void has not coalesced and the entire boundary is thermally insulated. If during the deformations of the body, any point on the void surface touches the vertical axis, the boundary condition on it is changed to (2.18). The boundary conditions (2.17) and (2.18) are due to the presumed symmetry of the deformations about the x_1 and x_2 axes. For the loading function $h(t)$ we take

$$\begin{aligned} h(t) &= v_0 t/t_r, \qquad 0 \leqq t \leqq t_r, \\ &= v_0, \qquad t > t_r, \end{aligned} \tag{2.20}$$

where $2H$ is the height of the block and v_0 is the steady speed of the top surface. The steady speed is reached in time t_r.

At the common interface between the matrix and the reinforcing layer, the velocity field, surface tractions, the temperature and the normal component of the heat flux are assumed to be continuous.

3 Computational considerations

Substitution for $\boldsymbol{T}$, $\boldsymbol{Q}$ and e from Eqs. (2.5) through (2.10) into the balance laws (2.2) and (2.3) results in coupled nonlinear partial differential equations which along with initial conditions (2.14) and boundary conditions (2.15) through (2.19) are to be solved for ϱ, $\boldsymbol{v}$ and θ. We use the updated Lagrangian method [42] to solve the problem. That is, in order to find the fields of ϱ, $\boldsymbol{v}$ and θ in the body at time $t + \Delta t$, the configuration of the body at time t is taken as the reference configuration. The governing nonlinear partial differential equations are first reduced to a set of coupled nonlinear ordinary differential equations by using the Galerkin approximation [42] and the lumped mass matrix. Figure 2 depicts the

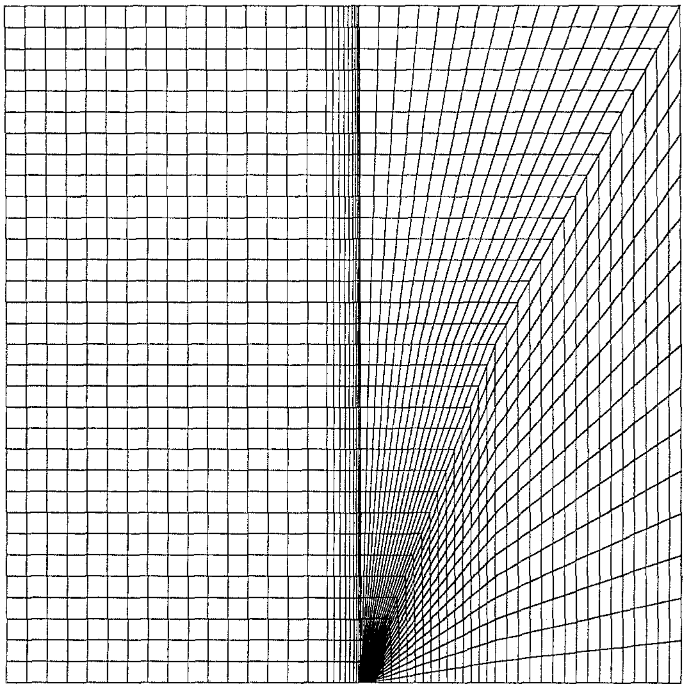

Fig. 2. The finite element discretization of the domain in the stress free reference configuration

discretization of the stress free reference configuration into 4-noded isoparametric quadrilateral elements that has been used to analyze the problem. The mesh is very fine in the region surrounding the void and gradually becomes coarse as we move away from it. The layer as well as a small matrix region adjoining it has been divided into a fine mesh too. We add that the coordinates of the nodes are updated after each time increment. Thus, the spatial domain occupied by the body and the shapes of these elements vary with time. At each node the mass density, two components of the velocity and the temperature are unknown. The coupled nonlinear ordinary differential equations are integrated by using the Gear method [43] for stiff differential equations. We use the subroutine LSODE taken from the package ODEPACK, developed by Hindmarsh [44], and employed the option of using the full Jacobian matrix. The subroutine adjusts the time step adaptively until a solution of the coupled nonlinear ordinary differential equations has been computed to the desired accuracy. The finite element code developed earlier by Batra and Liu [38] was modified to study the present problem.

4 Computation and discussion of results

We used the following values of various material and geometric parameters to compute results that are discussed below:

$$\begin{aligned} &b = 10{,}000 \text{ sec}, \ \sigma_0 = 333 \text{ MPa}, \ k = 49.22 \text{ W m}^{-1}\,{}^\circ\text{C}^{-1}, \ m = 0.025, \\ &c = 473 \text{ J kg}^{-1}\,{}^\circ\text{C}^{-1}, \ \varrho_0 = 7{,}860 \text{ kg m}^{-3}, \ B = 128 \text{ GPa}, \qquad (3.1) \\ &H = 5 \text{ mm}, \ v_0 = 25 \text{ m sec}^{-1}, \ \alpha = 0.0025\,{}^\circ\text{C}^{-1}. \end{aligned}$$

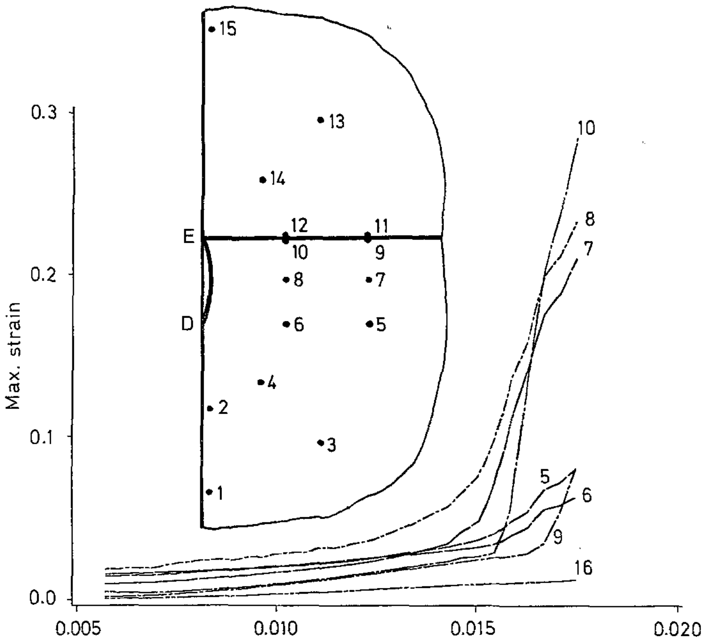

a

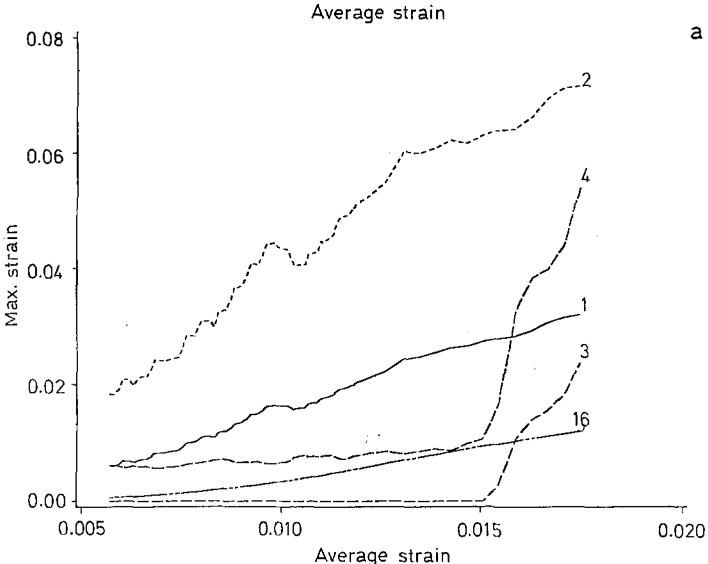

b

Fig. 3a. The maximum principal logarithmic strain versus the average strain at points 5 through 10 and 16 when the layer material is softer than the matrix material. Coordinates, in the stress free reference configuration, of these points are: 5 (0.0200, 0.4650), 6 (0.010, 0.4650), 7 (0.0200, 0.4700), 8 (0.010, 0.4700), 9 (0.0200, 0.4749), 10 (0.010, 0.4749), 16 (0.010, 0.8000)

Fig. 3b. The maximum principal logarithmic strain versus the average strain at points 1 through 4 and 16 when the layer material is softer than the matrix material. Coordinates, in the stress free reference configuration, of these points are: 1 (0.0010, 0.4450), 2 (0.0010, 0.4550), 3 (0.0141, 0.4509), 4 (0.0071, 0.4579)

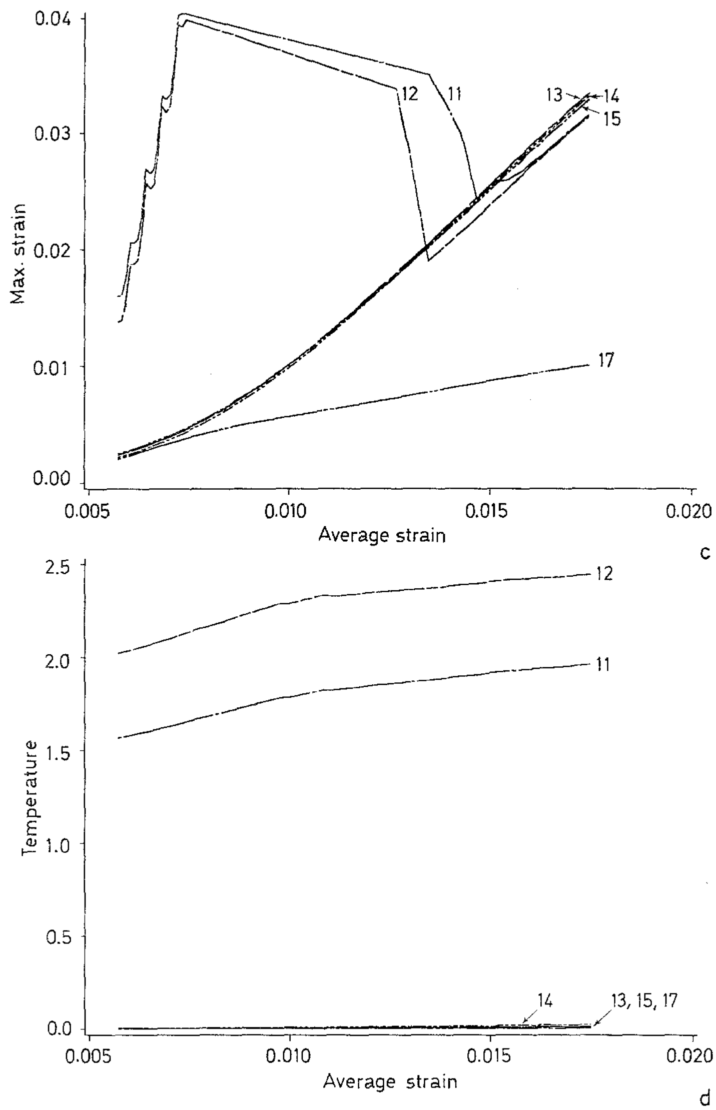

Fig. 3c. The maximum principal logarithmic strain versus the average strain at points 11 through 15 and 17 when the layer material is softer than the matrix material. All of these points are in the soft layer. Coordinates, in the stress free reference configuration, of these points are: 11 (0.0200, 0.4751), 12 (0.0100, 0.4751), 13 (0.01414, 0.4891), 14 (0.0071, 0.4821), 15 (0.0010, 0.5), 17 (0.5, 0.5)

Fig. 3d. The temperature rise versus the average strain at points 11 through 15 and 17 when the layer material is softer than the matrix material

Thus the average applied strain-rate $\dot{\gamma}_{avg}$ equals 5,000 sec^{-1}, $\theta_0 \equiv \sigma_0/(\varrho_0 c) = 89.6\,°\mathrm{C}$, and $\nu \equiv \varrho_0 v_0^2/\sigma_0 = 0.015$. The nondimensional number ν determines the effect of inertia forces relative to the flow stress of the material. For the simple shearing problem, Batra [21] noted that the inertia forces play a noticeable role when $\nu = 0.004$. Hence, the inertia forces will very likely play a significant role in the present problem.

We discuss below results in terms of the following nondimensional variables indicated by a superimposed bar.

$$\bar{\mathbf{s}} = \mathbf{s}/\sigma_0, \qquad \bar{\theta} = \theta/\theta_0, \qquad \bar{\boldsymbol{x}} = \boldsymbol{x}/H, \qquad \bar{I} = I/\dot{\gamma}_{avg}. \tag{3.2}$$

Henceforth, we drop the superimposed bars. To measure the deformation at a point, we use the maximum principal logarithmic strain ε given by

$$\varepsilon = \ln \lambda_1 \simeq -\ln \lambda_2, \tag{3.3}$$

where λ_1^2 and λ_2^2 are eigenvalues of the right Cauchy-Green tensor $C_{\alpha\beta} = x_{i,\alpha}x_{i,\beta}$ or the left Cauchy-Green tensor $B_{ij} = x_{i,\alpha}x_{j,\alpha}$. The second equality in Eq. (3.3) holds because the deformations of the body are nearly isochoric.

4.1 Layer material softer than the matrix material

Recall that one tip of the elliptical void is at the interface between matrix material and the relatively softer layer and the other tip is in the matrix. In order to find out where the shear bands form and their directions of propagation, we plot the evolution of the maximum principal logarithmic strain ε at several points surrounding the void and at points near the common interface between the layer and the matrix material. Figure 3a depicts the growth of ε at points 5 through 10 and point 16. Point 10 in the matrix is near the void tip that touches the common interface, point 9 is near the interface and on a horizontal line through point 10, point 8 is near the midsurface of the void and point 7 on a horizontal line through point 8, point 6 is near the other tip of the void and point 5 on a horizontal line through point 6. Point 16, not shown in the figure, is the near the vertical centroidal axis but is far removed from the void and the layer/matrix interfaces. Coordinates of these points in the stress free reference configuration are given in the figure caption and their approximate locations are shown in Fig. 3a. Results plotted in this figure clearly indicate that at a nominal strain of nearly 0.015, the values of ε at points 7, 8 and 10 increase sharply with the rate of growth of ε at point 10 being higher than that at points 7 and 8. Note that the value of ε at point 16 is very close to the average strain, and the values of ε at points 5, 6 and 9 are higher than that at point 16 but considerably smaller than those at points 7,8 and 10. Thus the small region containing points 7, 8 and 10 undergoes severe deformations. In Fig. 3b, we have plotted the growth of ε at points 1, 2, 3, 4 and 16. Point 2 is near the void tip D, point 1 is on a vertical line through point 2, and the line joining points D, 4 and 3 makes an angle of 45° with the vertical. At an average strain of approximately 0.015, the values of ε at points 3 and 4 increase sharply. However, the peak values attained at points 1, 2, 3 and 4 are much lower than those at points 7, 8 and 10. Thus in the matrix material surrounding the void, more intense deformations occur near the void tip E at the matrix/layer interface. In an attempt to assess the deformations of the layer, we have plotted ε versus the average strain in Fig. 3c at points 11, 12, 13, 14, 15 and 17 in the layer. Points 11 and 12 are near the matrix/layer interface and correspond respectively to points 9 and 10 in the matrix, the line joining points E, 14 and 13 makes an angle of 45° with the horizontal, point 15 is near the vertical centroidal axis, and point 17 in the layer is far removed from the void tip. The approximate location of these points is given in Fig. 3a and their coordinates in the stress free reference configuration are given in the figure caption. Even though the values of ε at points 11 and 12 increase sharply in the beginning, they eventually match those at points 13, 14 and 15. Recalling that σ_0 for the layer material equals one—fifth that for the matrix material, we may imagine the void to be in a rigid material as far as the deformations of the layer are concerned. Thus the deformations of the layer near the void tip need not be excessively large as compared to its average deformations. This is borne out by the results plotted in Fig. 3c which show that the peak values of ε at points 13, 14 and 15 are nearly twice the average. Because of the continuity of the displacements and temperatures across the layer/matrix interface, initially points 11 and 12 undergo essentially the same deformations as points 9 and 10. The rise in the temperature at points 11 and 12 makes the material there softer. The surrounding relatively hard layer material results in redistribution of the deformations. Note that points 9, 10, 11 and 12 are a little bit away from the layer/matrix interface. Thus one may conclude that no localization of the deformation into a shear band occurs within the layer material near the void tip. That the temperature rise at points 11 and 12 is much larger than that at points 13, 14, 15 and 17 becomes clear from the results plotted in Fig. 3d. The plots of the temperature rise at other points considered are not included herein. However, we note that the temperature rise at points 7, 8 and 10 where severe deformations of the matrix material occur was considerably more than that at point 16 which is far away from the void.

We now focus on the deformations of the layer and the matrix materials near points P and Q on the right traction free surface. Points P and Q are also on the layer/matrix interfaces. Figure 4a shows the plot of ε versus the average strain at points 18 through 25 near the upper matrix/layer interface. Points 18 through 21 are in the layer and points 22 through 25 are in the matrix. It is clear that deformations of points 18 and 19 are significantly more than the deformations of other points considered in this plot. Also intense deformations of the layer material surrounding point 18 propagate horizontally to point 19. The deformations of points 21 through 25 are very small as compared to the deformations of points 18 and 19. The value of ε at point 20 is nearly four times that at point 21. It is possible that the intense deformations initiating at point 18 propagate to point 20 too. In an attempt to shed some light on what happens to the shear band initiating from point 18, we have plotted in Fig. 4b values of ε versus the average strain at points 24 through 30 in the matrix. Points 20, 24, 27 and 29 are on the same vertical line with points 20 and 24 on the opposite sides of the matrix layer/interface. Points 24, 27 and 29 are in the matrix. Points 24, 26 and 25 are on a horizontal line and points 24, 28 and 30 are on the line that makes an angle of 45° with the horizontal. Relatively large values of ε at points 24, 26, 27, 28 and 30 seem to suggest that the region surrounding points 24, 26 and 27 deforms severely and that these severe deformations propagate along the line joining points 24, 28 and 30. Since points 20 and 24 are very near to each other, it is reasonable to conclude that the localization of deformation initiating at point 18 within the soft layer propagates towards point 20 and then along the line joining points 20, 28 and 30. Results plotted at similarly situated points near the other interface between the layer and the matrix reveal that a shear band initiating from point Q propagates horizontally within the layer too and then into the matrix along a line that makes an angle of 45° with the vertical.

The picture of the development of shear bands outlined above is reinforced by the plots of contours of ε shown in Fig. 5 at three values of the average strain. One shear band initiates within the matrix surrounding the void tip near the matrix/layer interface and

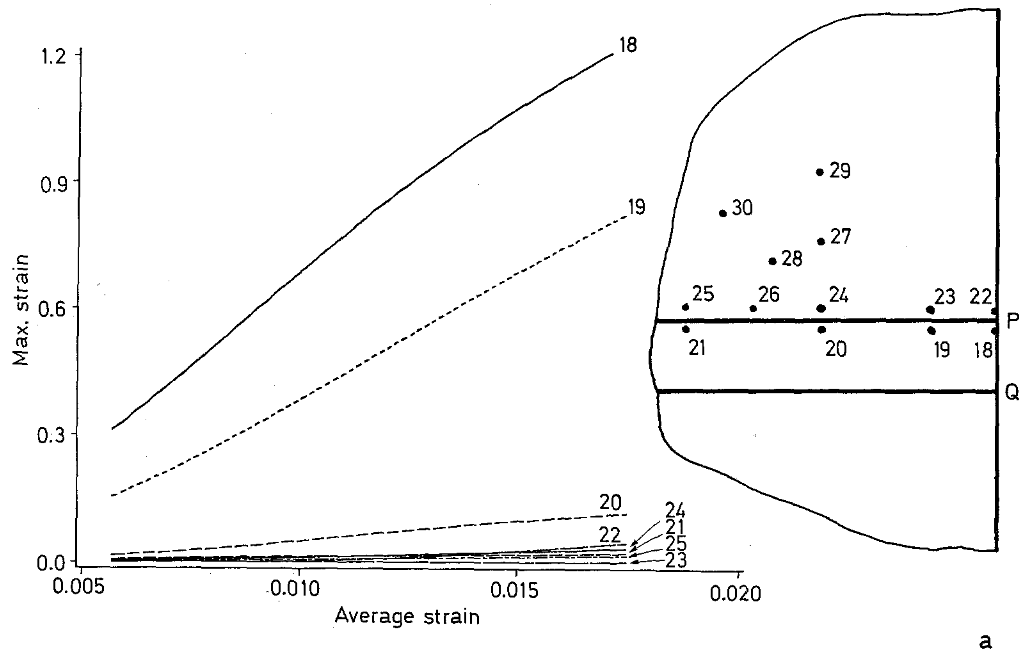

Fig. 4a. The maximum principal logarithmic strain versus the average strain at points 18 through 25 when the layer material is softer than the matrix material. Coordinates of these points in the stress free reference configuration are: 18 (0.999, 0.522), 19 (0.95, 0.522), 20 (0.87, 0.522), 21 (0.77, 0.522), 22 (0.999, 0.532), 23 (0.95, 0.532), 24 (0.87, 0.532), 25 (0.77, 0.532)

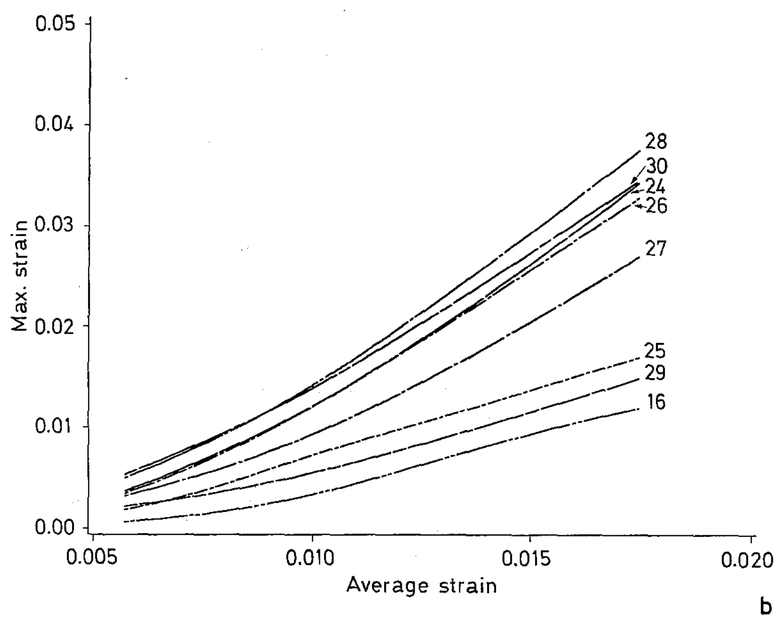

Fig. 4b. The maximum principal logarithmic strain versus the average strain at points 24 through 30 and 16 when the layer material is softer than the matrix material. Coordinates of points not given earlier are: 26 (0.82, 0.532), 27 (0.87, 0.582), 28 (0.8346, 0.5674), 29 (0.87, 0.632), 30 (0.7993, 0.6027)

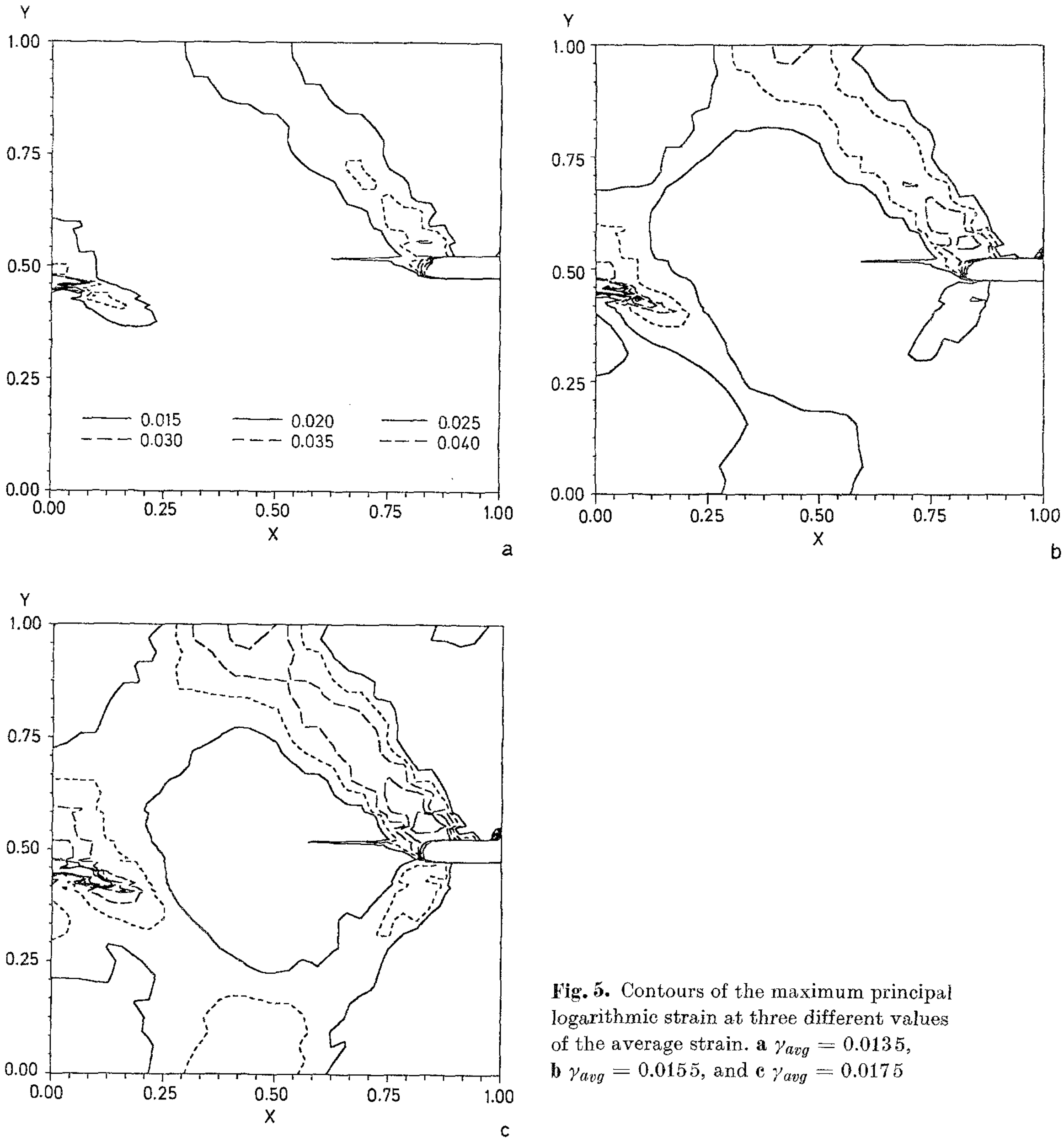

Fig. 5. Contours of the maximum principal logarithmic strain at three different values of the average strain. **a** $\gamma_{avg} = 0.0135$, **b** $\gamma_{avg} = 0.0155$, and **c** $\gamma_{avg} = 0.0175$

propagates into the matrix material below the common interface, the direction of propagation being nearly 45° to the vertical axis. The shear bands initiating at points of intersection of the matrix/layer interfaces with the right traction free surface propagate into the soft layer and then bifurcate into the matrix material along lines making an angle of approximately 45° with the vertical. The band in the layer near the upper matrix/layer interface bifurcates into the matrix prior to that near the lower interface. Also the band in the layer near the upper matrix/layer interface continues to propagate horizontally into the layer too while that near the lower surface does not. In order to elucidate upon the differences between these two bands within the soft layer, we have plotted in Figs. 6a, 6b and 6c contours of ε and in Figs. 6d, 6e and 6f contours of the temperature rise θ in a

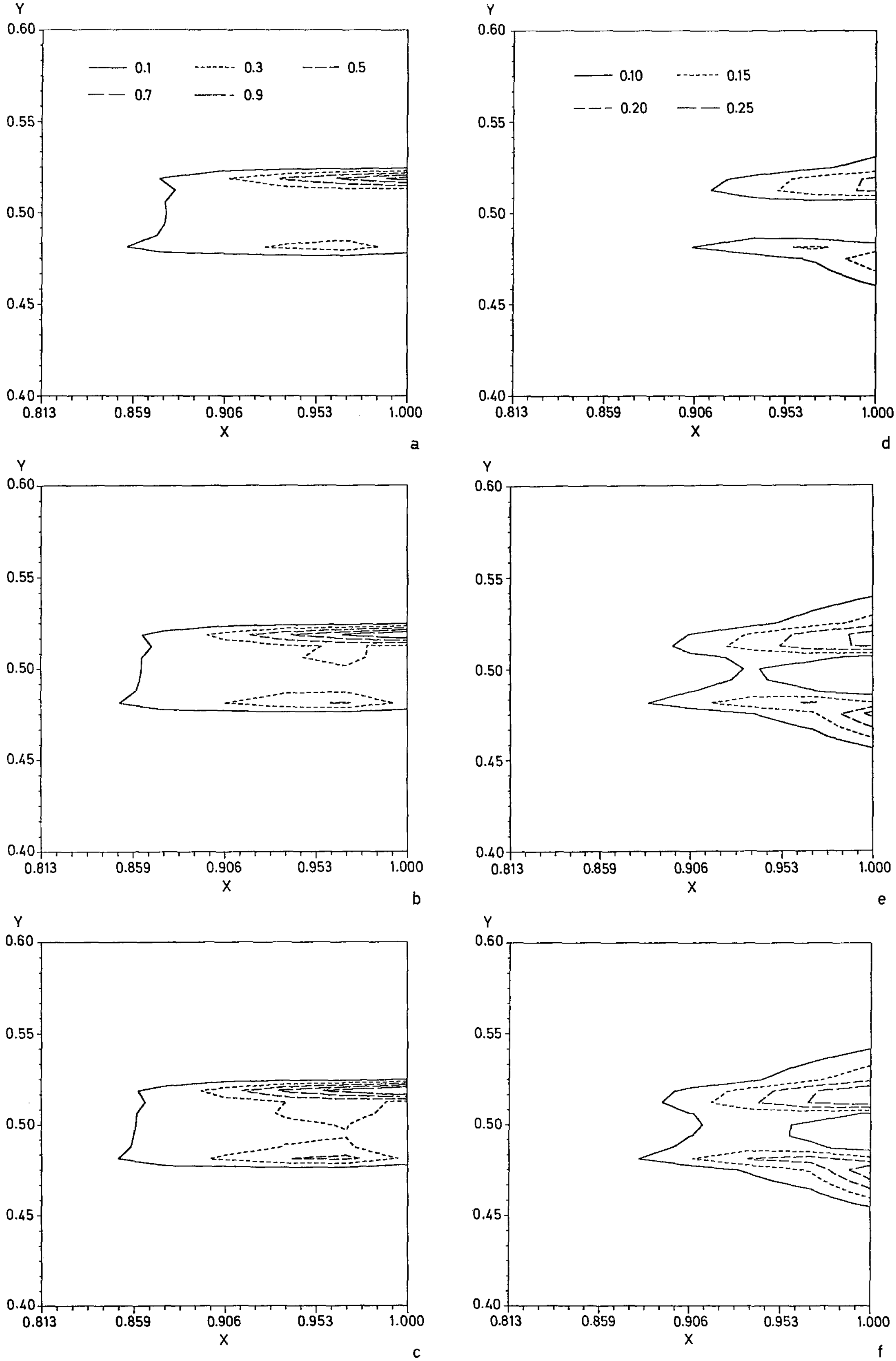

Y
0.60
0.55
0.50
0.45
0.40
0.813
0.859
0.906
0.953
1.000
X
0.1
0.3
0.5
0.7
0.9
a
b
c
0.10
0.15
0.20
0.25
d
e
f

small region surrounding the layer and near the right traction-free surface. We note that the layer material near the upper interface undergoes more severe deformations than the layer material near the lower interface. This could be due to the differences in the reflection and refraction of waves at the two interfaces, and the interaction of these waves with the loading wave. The bands near the upper and lower interfaces propagate both horizontally in the layer and laterally towards each other. Had the computations been carried further, it is clear that the two bands will merge with each other. The computations could not be carried further because we had exhausted the computing resources available to us. Because of the stiff equations and the nonuniform mesh, the time step required to integrate the equations is extremely small. The contours of θ indicate that the matrix material is also being heated up. Since the layer is softer than the matrix material, the stress in it is low and higher values of ε in the layer give rise to nearly the same value of the energy dissipated as the lower values of ε in the matrix because the stress in it is higher. The temperature rise makes the matrix material softer and the bands propagating in the layer bifurcate into two, one travels horizontally into the layer and the other into the matrix material along the direction of the maximum shear stress.

Figure 7 shows the distribution of the vertical component of the velocity at an average strain of 0.0175. In our work the velocity field is assumed to be continuous throughout the

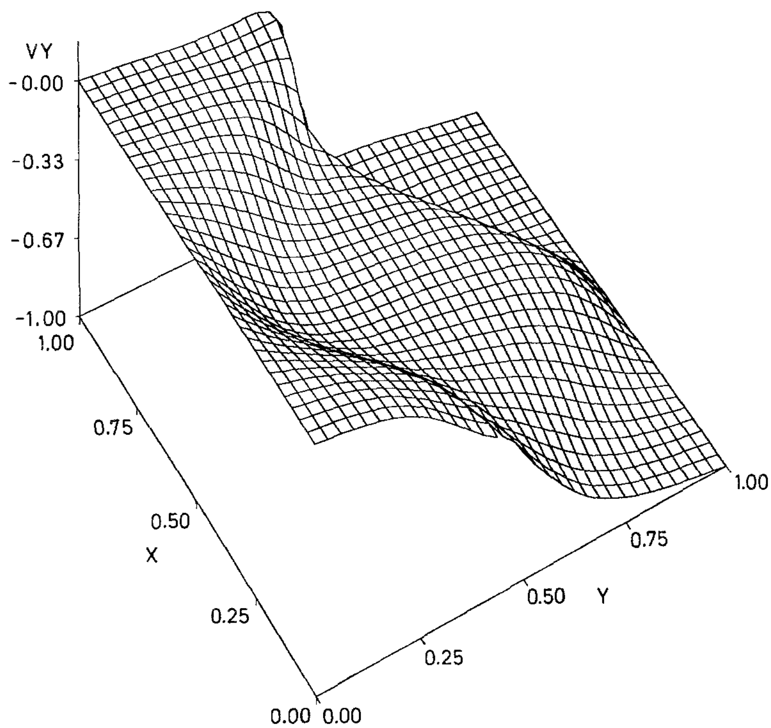

Fig. 7. Distribution of the vertical component of the velocity in the cross-section when the layer material is softer than the matrix material at $\gamma_{avg} = 0.0175$

←

Fig. 6. Contours of the maximum principal logarithmic strain and temperature rise within a small region enclosing the soft layer near the right traction-free surface at three different values of the average strain. **a, d** $\gamma_{avg} = 0.0135$, **b, e** $\gamma_{avg} = 0.0163$, and **c, f** $\gamma_{avg} = 0.0175$

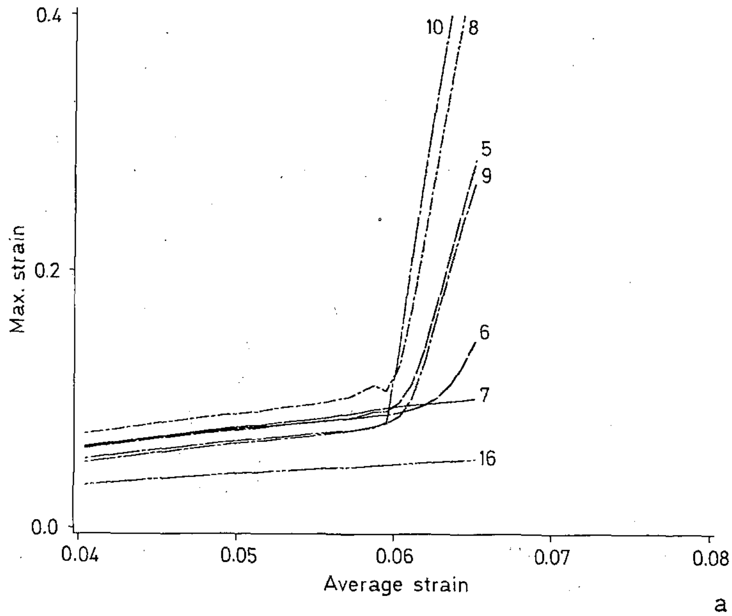

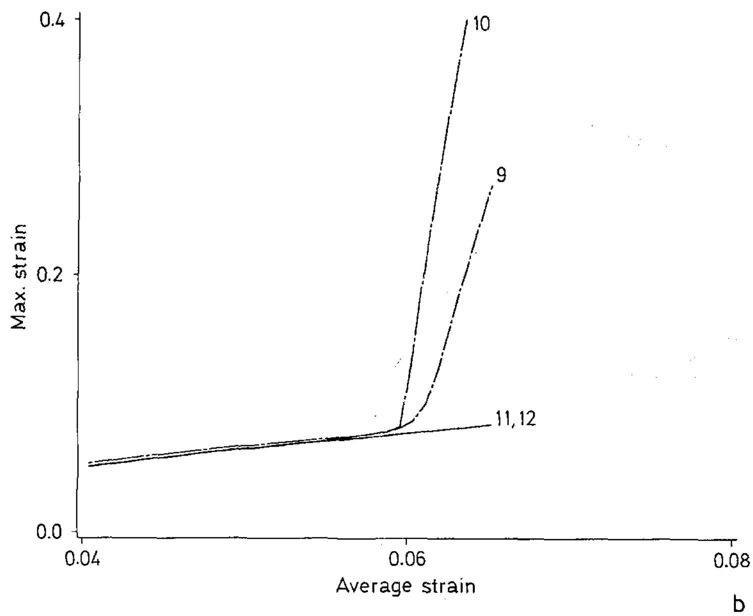

Fig. 8a. The maximum principal logarithmic strain versus the average strain at points 5 through 10 and 16 when the layer material is stronger than the matrix material. Coordinates of these points in the stress free reference configuration are the same as for points in Fig. 3a and are given in the caption of Fig. 3a.

Fig. 8b. The maximum principal logarithmic strain versus the average strain at points 9, 10, 11 and 12 when the layer material is stronger than the matrix material. Coordinates of these points in the stress free reference configuration are given in the captions of Figs. 3a and 3c.

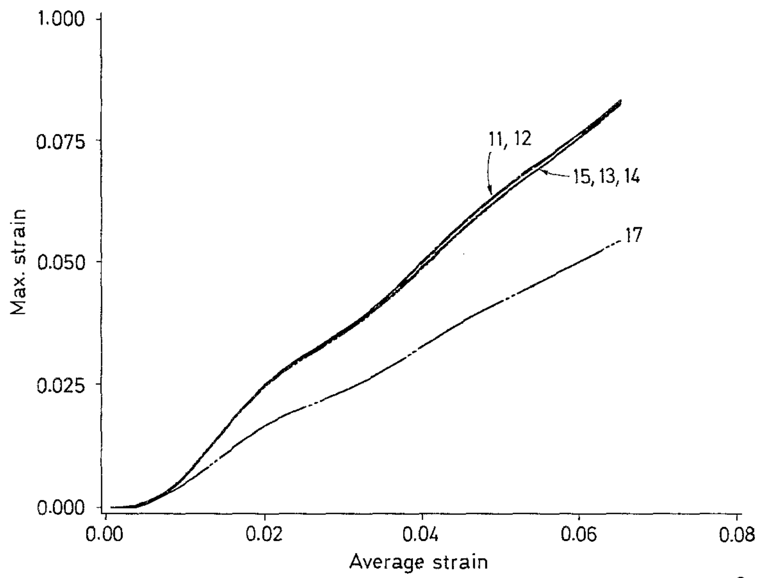

c

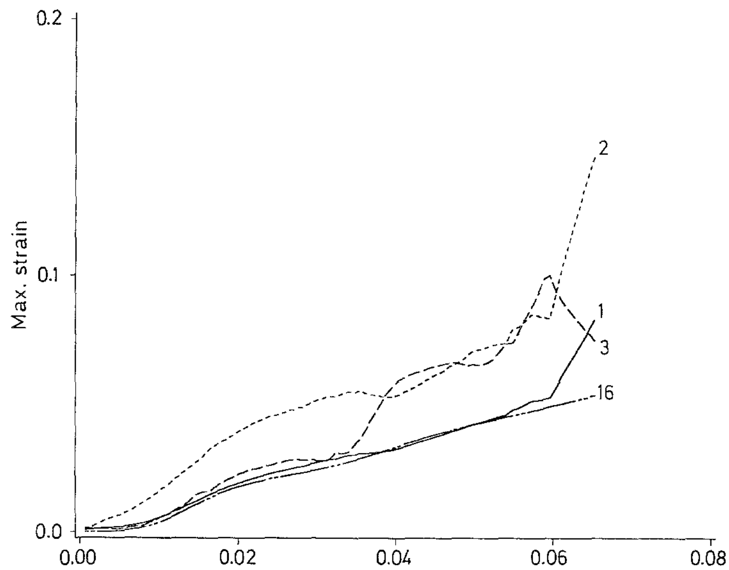

d

Fig. 8c. The maximum principal logarithmic strain versus the average strain at points 11 through 15 and point 17 when the layer material is stronger than the matrix material. See Figs. 3a and 3c for the coordinates of these points in the stress free reference configuration.

Fig. 8d. The maximum principal logarithmic strain versus the average strain at points 1, 2, 3 and 16 when the layer material is stronger than the matrix material. See Fig. 3a and 3b for the coordinates of these points in the stress free reference configuration.

region. However, the plotted velocity field does show that the value of v_2 increases sharply as one crosses the severely deforming region thus supporting the assertions made by Tresca [2] and Massey [3].

4.2 *Layer material stronger than the matrix material*

Figures 8a, 8b and 8c depict the growth of the maximum principal logarithmic strain ε at several matrix points near the void. The coordinates of these points in the stress free reference configuration are given in the figure captions and their approximate locations are shown in Fig. 3a. Results plotted in Fig. 8a clearly indicate that at a nominal strain of

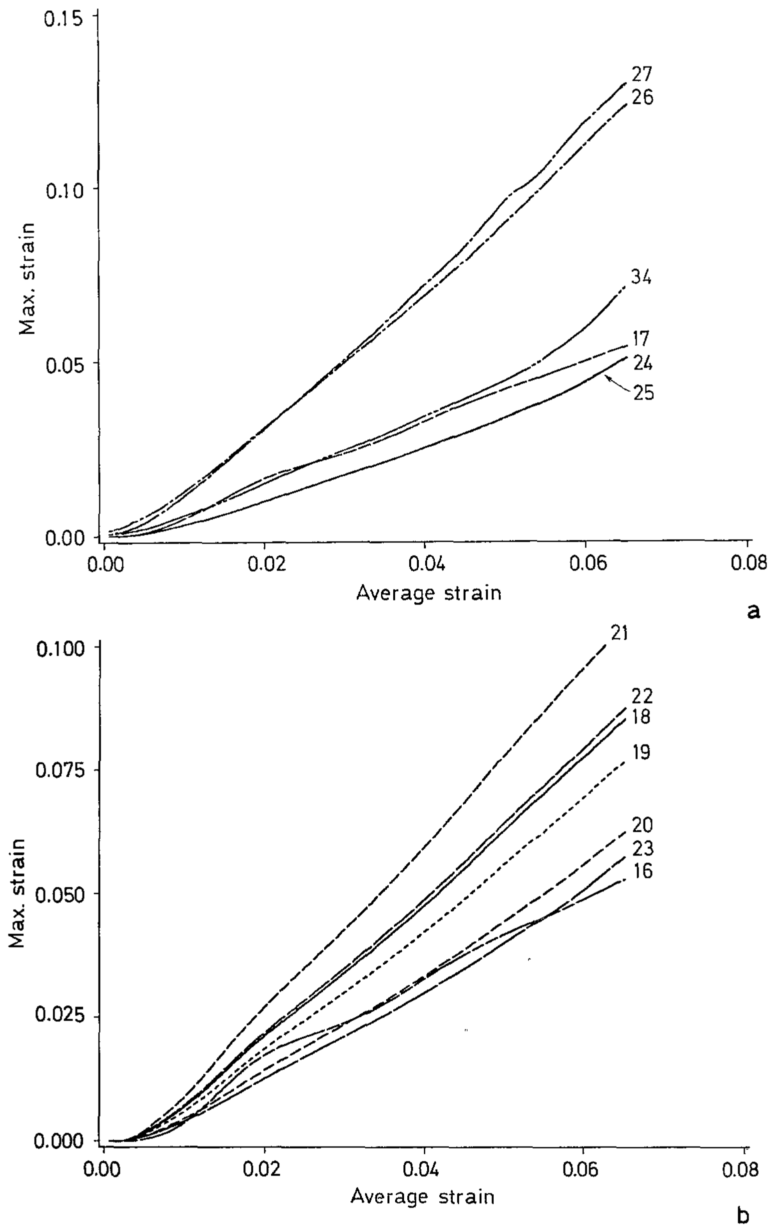

Fig. 9

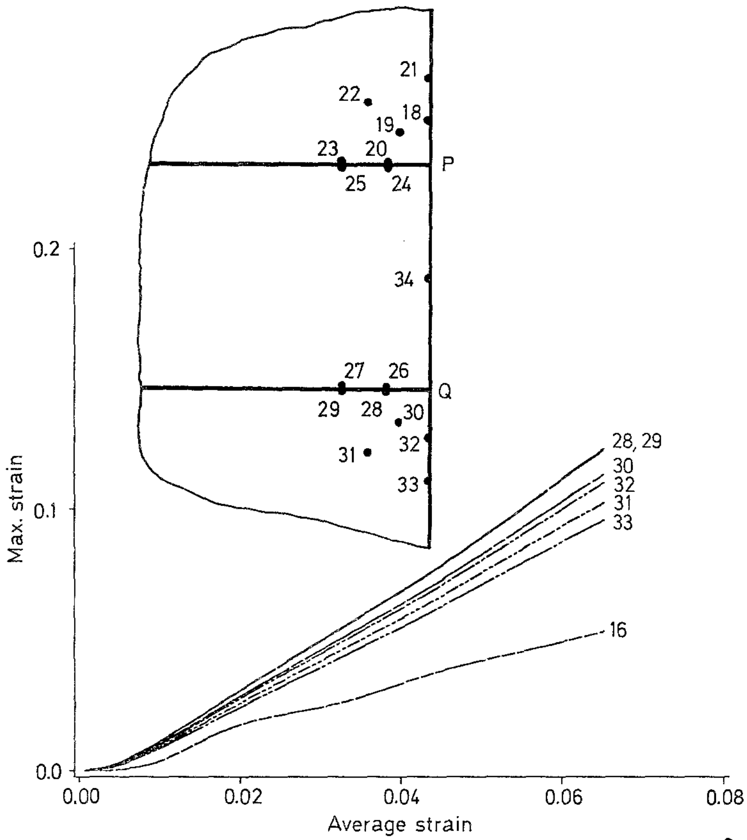

c

Fig. 9. The maximum principal logarithmic strain versus the average strain at points 18 through 34 when the layer material is stronger than the matrix material. Coordinates of these points in the stress free reference configuration are: 18 (0.999, 0.535), 19 (0.993, 0.5321), 20 (0.990, 0.5251), 21 (0.999, 0.545), 22 (0.9859, 0.5391), 23 (0.980, 0.5251), 24 (0.990, 0.5249), 25 (0.98, 0.5249), 26 (0.99, 0.4751), 27 (0.98, 0.4751), 28 (0.99, 0.4749), 29 (0.98, 0.4749), 30 (0.993, 0.4679), 31 (0.9859, 0.4609), 32 (0.999, 0.465), 33 (0.999, 0.455), 34 (0.999, 0.5)

0.06, the values of ε at points 5, 8, 9 and 10 increase sharply, with the rate of growth of ε at points 8 and 10 being much greater than that at points 5 and 9. Thus the small region containing points 8, 9 and 10 undergoes intense deformations which propagate towards point 5. This will become transparent when we subsequently plot the contours of ε. Recall that point 10 is near the void tip that touches the matrix/layer interface, point 9 is near the interface and on a horizontal line through point 10, point 8 is near the midsurface of the void, points 7 and 8 are on a horizontal line, point 6 is near the other void tip, and point 5 on a horizontal line through point 6. Because the layer material is harder than the matrix material, the maximum principal logarithmic strain ε at points 11 and 12 adjoining points 9 and 10 respectively is considerably less than that at points 9 and 10. The values of ε versus the average strain at these four points are shown in Fig. 8b. In Fig. 8c, we have plotted the evolution of ε at points 11 through 17 in the layer. Points 13 and 14 are on a line through the void tip that makes an angle of 45° with the horizontal, point 15 is near the vertical centroidal axis, and point 17 is on the midsurface of the layer but far removed from the void tip. At an average strain of 0.06, the values of ε at points 11 through 15 are nearly 40% higher than that at point 17 and this difference increases

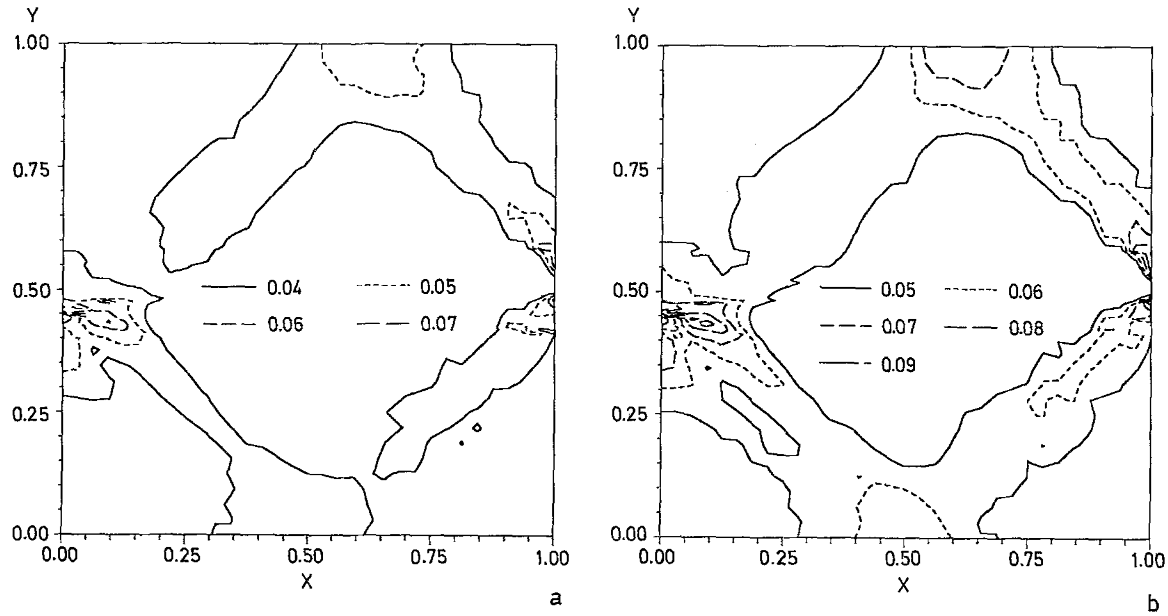

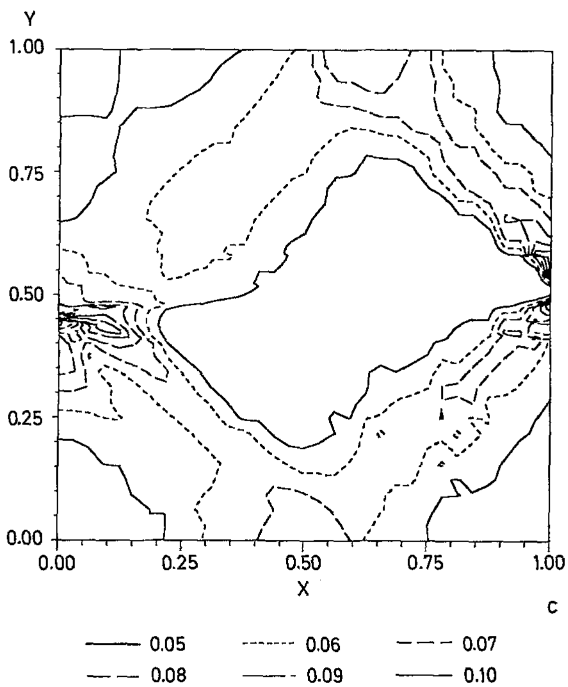

Fig. 10. Contours of the maximum principal logarithmic strain at three different values of the average strain when the layer material is stronger than the matrix material.
a $\gamma_{avg} = 0.0388$, **b** $\gamma_{avg} = 0.05$, **c** $\gamma_{avg} = 0.0572$

with increase in the average strain. Since points 11 through 15, distributed in the layer region surrounding the void tip, have undergone the same amount of deformation, it is reasonable to conclude that no localization of deformation has occurred in the layer. The plot of ε versus the average strain at points 1, 2, 3 and 16, depicted in Fig. 8d, reveals that at an average strain of approximately 0.06, the small region surrounding point 2 deforms severely and these deformations propagate towards point 1. We note that point 2 is near the void tip away from the matrix/layer interface, and points 1 and 2 are near the vertical centroidal axis.

In the previous case when the layer material was weaker than the matrix material, a shear band formed at an average strain of 0.016. In that case, the layer material underwent severe deformations. However, because of the small thickness of the layer, the overall deformations of the body stayed small.

We now explore deformations of the layer and matrix materials surrounding points P and Q on the right traction-free edge of the block. The coordinates of the selected points in the stress free reference configuration are given in the figure captions, and their approximate locations are shown in Fig. 9c. Results plotted in Figs. 9a, 9b and 9c reveal that the growth of ε at any one of these points is not phenomenal as compared to the average strain either in the layer (e.g. at point 17), or in the block (e.g. at point 16), or the overall average strain. At an average strain of 0.06, the values of ε at points 26 and 27 in the layer equal 2.5 times that at point 17, but that at layer points 24 and 25 which are near the upper layer interface, are comparable to the value of ε at point 17. The values of ε at matrix points situated below the matrix/layer interface are higher than those at similarly situated matrix points above the matrix/layer interface. Thus the shear band initiating from point Q and propagating into the matrix material will involve more severe deformations than that initiating from point P and propagating into the matrix. Unlike the case of the soft layer, the deformations within the layer do not localize into a shear band.

Figure 10 depicts contours of ε at $\gamma_{avg} = 0.0388$, 0.05, and 0.0572. These reveal that a shear band initiating from the void tip abutting the matrix/layer interface propagates initially along the interface and then into the matrix material along a line making an angle of nearly 45° with the vertical. The shear band initiating from the lower void tip also propagates into the matrix material along a line making an angle of approximately 45° with the vertical. Two shear bands also initiate from points P and Q on the right traction free surface and these propagate into the matrix material along lines making an angle of 45° with the vertical. Even though it seems that near the vertical centroidal axis a shear band has propagated into the layer, there is no localization of the deformation occurring in the layer material. This is evidenced by the plots of ε versus the average strain at several points in the layer that are included in Fig. 8c. Even though the strain within the layer is small, the values of stress are not and the total energy dissipated at a layer particle may be comparable to that at a matrix particle. The contours of the temperature rise, not included in the paper, support the picture laid out above for the development of four bands, two from the void tips and two from points on the right traction free surface where the layer and the matrix materials meet.

5 Conclusions

We have studied plane strain thermomechanical deformations of a thermally softening viscoplastic body of square cross-section and containing two elliptical voids and two thin layers placed symmetrically about the horizontal centroidal axis. The major axes of the voids are aligned with the vertical centroidal axis of the cross-section and one tip of each void touches the matrix/layer interface. Two cases, namely when the flow stress in a quasistatic simple compression test for the layer material equals one-fifth or five times that of the matrix material, are studied. When the layer material is weaker than the matrix material, two bands initiate from points on the vertical traction free surfaces where the layer and the matrix materials meet. These bands propagate horizontally into the layer and also spread out laterally towards each other. The band near the upper layer/matrix interface is stronger than the one near the lower layer/matrix interface in the sense that the peak value of the maximum principal logarithmic strain in it is higher than that in the band near the lower layer/matrix interface. These bands eventually cross the interface and propagate into the matrix material along the direction of the maximum shearing stress. The band near the upper layer/matrix interface continues to propagate horizontally too. The matrix material surrounding the void tip touching the layer/matrix interface undergoes severe deformations also. This band initially propagates horizontally along the interface for a small distance and then propagates into the matrix material in the direction of the maximum shearing stress.

When the layer material is stronger than the matrix material, two bands initiate from points on the vertical traction free surfaces where the layer/matrix interfaces intersect them. These bands propagate into the matrix along the direction of the maximum shearing stress. Also bands initiate from each of the void tips. The bands initiating from the void tips touching the matrix/layer interfaces initially propagate horizontally and then into the matrix material in the direction of the maximum shearing stress. The bands initiating from the other void tips also propagate into the matrix material in the direction of the maximum shearing stress. In this case no localization of deformation occurs within the layer. The average strain at which a shear band forms in this case is nearly four times that in the previous case of softer layer material.

Acknowledgements

This work was supported by the U.S. National Science Foundation Grant MSM 8715952 and the U.S. Army Research Office Contract DAAL03-88-K-0184 to the University of Missouri-Rolla.

References

[1] Johnson, W.: Henri Tresca as the originator of adiabatic heat lines. Int. J. Mech. Sci. **29**, 301–310 (1987).
[2] Tresca, H.: On further application of the flow of solids. Proc. Inst. Mech. Engr. **30**, 301–345 (1878).
[3] Massey, H. F.: The flow of metal during forging. Proc. Manchester Assoc. Engineers, pp. 21–26 (1921). Reprinted by the National Machinery Co., Tiffon, Ohio (1946).
[4] Zener, C., Hollomon, J. H.: Effect of strain rate on plastic flow of steel. J. Appl. Phys. **14**, 22–32 (1944).
[5] Moss, G. L.: Shear strain, strain rate and temperature changes in an adiabatic shear band. In: Shock waves and high strain rate phenomenon in metals (Meyer, M. A., Murr, L. E., eds.), pp. 299–312. New York: Plenum Press 1981.
[6] Costin, L. S., Crisman, E. E., Hawley, R. H., Duffy, J.: On the localization of plastic flow in mild steel tubes under dynamic torsional loading. Int. Phys. Conf. Ser. No. **47**, 90–100 (1979).
[7] Hartley, K. A., Duffy, J., Hawley, R. H.: Measurement of the temperature profile during shear band formation in steels deforming at high strain rates. J. Mech. Phys. Solids **35**, 283–301 (1987).
[8] Giovanola, J. H.: Adiabatic shear banding under pure shear loading. Part I. Direct observation of strain localization and energy dissipation measurements. Mech. Materials **7**, 59–71 (1988).
[9] Marchand, A., Duffy, J.: An experimental study of the formation process of adiabatic shear bands in a structural steel. J. Mech. Phys. Solids **36**, 251–283 (1988).
[10] Wright, T. W., Walter, J. W.: On stress collapse in adiabatic shear bands. J. Mech. Phys. Solids **35**, 701–716 (1987).
[11] Molinari, A., Clifton, R. J.: Analytic characterization of shear localization in thermoviscoplastic materials. ASME J. Appl. Mech. **54**, 806–812 (1987).

[12] Batra, R. C., Kim, C. H.: Adiabatic shear banding in elastic-viscoplastic nonpolar and dipolar materials. Int. J. Plasticity **6**, 127—141 (1990).
[13] Batra, R. C., Kim, C. H.: Effect of viscoplastic flow rules on the initiation and growth of shear bands at high strain rates. J. Mech. Phys. Solids **38** (in press).
[14] Batra, R. C., Kim, C. H.: Analysis of shear banding in six ductile metals. Submitted for publication.
[15] Batra, R. C., Kim, C. H.: Analysis of shear banding in six less ductile metals. Submitted for publication.
[16] Wright, T. W., Batra, R. C.: The initiation and growth of adiabatic shear bands. Int. J. Plasticity **1**, 205—212 (1985).
[17] Wright, T. W., Batra, R. C.: Adiabatic shear bands in simple and dipolar plastic materials. In: Proc. IUTAM Symposium on Macro-Micro-Mechanics of High Velocity Deformation and Fracture (Kawata, K., Shioiri, J., eds.), pp. 189—201. Berlin—Heidelberg—New York: Springer 1987.
[18] Clifton, R. J., Duffy, J., Hartley, K. S., Shawki, T. G.: On critical conditions for shear band formation at high strain rates. Scripta Metallurgica **18**, 443—448 (1984).
[19] Batra, R. C.: The initiation and growth of, and the interaction among adiabatic shear bands in simple and dipolar materials. Int. J. Plasticity **3**, 75—89 (1987).
[20] Batra, R. C.: Effect of material parameters on the initiation and growth of adiabatic shear bands. Int. J. Solids and Structures **23**, 1435—1446 (1987).
[21] Batra, R. C.: Effect of nominal strain-rate on the initiation and growth of adiabatic shear bands. ASME J. Appl. Mech. **55**, 229—230 (1988).
[22] Merzer, A. M.: Modeling of adiabatic shear band development from small imperfections. J. Mech. Phys. Solids **30**, 323—338 (1982).
[23] Wu, F. H., Freund, L. B.: Deformation trapping due to thermoplastic instability in one-dimensional wave propagation. J. Mech. Phys. Solids **32**, 119—132 (1984).
[24] Burns, T.: A mechanism for shear band formation in the high strain rate torsion test. J. Appl. Mech. (in press).
[25] Fressengeas, C.: Adiabatic shear morphology at very high strain rates. Int. J. Impact Engr. 8, 141—157 (1989).
[26] Recht, R. F.: Catastrophic thermoplastic shear. ASME J. Appl. Mech. **31**, 189—193 (1964).
[27a] Staker, M. R.: The relation between adiabatic shear instability strain and material properties. Acta Met. **29**, 683—689 (1981).
[27b] Burns, T. J.: Approximate linear stability analysis of a model of adiabatic shear band formation. Quart. Appl. Math. **43**, 65—84 (1985).
[28] Clifton, R. J.: Adiabatic shear banding. In: Material response to ultrahigh loading rates, chapter 8, pp. 129—142. NRC National Material Advisory Board (U.S.) Report No. NMAB-356.
[29] Coleman, B. D., Hodgdon, M. L.: On shear bands in ductile materials. Arch. Rat. Mech. Anal. **90**, 219—247 (1985).
[30] Wright, T. W.: Steady shearing in a viscoplastic solid. J. Mech. Phys. Solids **35**, 269—282 (1987).
[31] Anand, L., Kim, K. H., Shawki, T. G.: Onset of shear localization in viscoplastic solids. J. Mech. Phys. Solids. **35**, 381—399 (1987).
[32] Bai, Y. L.: A criterion for thermoplastic shear instability. In: Shock waves and high strain rate phenomenon in metals (Meyers, M. A., Murr, L. E., eds.) pp. 277—283. New York: Plenum Press 1981.
[33] LeMonds, J., Needleman, A.: Finite element analyses of shear localization in rate and temperature dependent solids. Mech. Materials **5**, 339—361 (1986).
[34] LeMonds, J., Needleman, A.: An analysis of shear band development incorporating heat conduction. Mech. Materials **5**, 363—373 (1986).
[35] Needleman, A.: Dynamic shear band development in plane strain. ASME J. Appl. Mech. **56**, 1—9 (1989).
[36] Zbib, H. M., Aifantis, E. C.: On the localization and postlocalization behavior of plastic deformation. I. On the initiation of shear bands. Res Mechanica **23**, 261—277 (1988).
[37] Anand, L., Lush, A. M., Kim, K. H.: Thermal aspects of shear localization in viscoplastic solids. In: Thermal aspects in manufacturing (Attia, M. H., Kops, L., eds.). ASME-PED **30**, 89—103 (1988).
[38] Batra, R. C., Liu, D. S.: Adiabatic shear banding in plane strain problems. ASME J. Appl. Mech. **56**, 527—534 (1989).

[39] Batra, R. C., Liu, D. S.: Adiabatic shear banding in dynamic plane strain compression of a viscoplastic material. Int. J. Plasticity **6**, 231—246 (1990).
[40] Zhu, Z. G., Batra, R. C.: Dynamic shear band development in plane strain compression of a viscoplastic body containing a rigid inclusion. Acta Mechanica **84**, 89—107 (1990).
[41] Batra, R. C., Zhang, X.-T.: Shear band development in dynamic loading of a viscoplastic cylinder containing two voids. Acta Mechanica **85**, 221—234 (1990).
[42] Bathe, K. J.: Finite element procedures in engineering analysis. Englewood Cliffs: Prentice-Hall 1982.
[43] Gear, C. W.: Numerical initial value problems in ordinary differential equations. Englewood Cliffs: Prentice-Hall 1971.
[44] Hindmarsh, A. C.: ODEPACK, A systematized collection of ODE solvers. In: Scientific computing (Stepleman, R. S. et al., eds.) pp. 55—64. Amsterdam: North-Holland 1983.

Authors' address: R. C. Batra and Z. G. Zhu, Department of Mechanical and Aerospace Engineering and Engineering Mechanics, University of Missouri-Rolla, Rolla, MO 65401-0249, U.S.A.